

Alternative method for determining the constant offset in lidar signal

Vladimir A. Kovalev,* Cyle Wold, Alexander Petkov, and Wei Min Hao

United States Forest Service, Rocky Mountain Research Station, Fire Sciences Laboratory,
5775 Highway 10 West, Missoula, Montana 59808, USA

*Corresponding author: vkovalev@fs.fed.us

Received 2 January 2009; revised 31 March 2009; accepted 14 April 2009;
posted 14 April 2009 (Doc. ID 105678); published 28 April 2009

We present an alternative method for determining the total offset in lidar signal created by a daytime background-illumination component and electrical or digital offset. Unlike existing techniques, here the signal square-range-correction procedure is initially performed using the total signal recorded by lidar, without subtraction of the offset component. While performing the square-range correction, the lidar-signal monotonic change due to the molecular component of the atmosphere is simultaneously compensated. After these corrections, the total offset is found by determining the slope of the above transformed signal versus a function that is defined as a ratio of the squared range and two molecular scattering components, the backscatter and transmittance. The slope is determined over a far end of the measurement range where aerosol loading is zero or, at least, minimum. An important aspect of this method is that the presence of a moderate aerosol loading over the far end does not increase dramatically the error in determining the lidar-signal offset. The comparison of the new technique with a conventional technique of the total-offset estimation is made using simulated and experimental data. The one-directional and multiangle measurements are analyzed and specifics in the estimate of the uncertainty limits due to remaining shifts in the inverted lidar signals are discussed. The use of the new technique allows a more accurate estimate of the signal constant offset, and accordingly, yields more accurate lidar-signal inversion results. © 2009 Optical Society of America

OCIS codes: 280.3640, 290.1350, 290.2200.

1. Introduction

The original signal recorded by lidar is the total of the attenuated range-dependent backscatter signal and the constant offset. The offset is created by a background constituent, the level of which depends on the background luminance, the lidar optics and recording system parameters, and by electronic offset originated during the amplification and digitization of the detected signal.

The retrieval of optical characteristics of the aerosol particulates from the recorded lidar signal requires accurate evaluation of all parameters, atmospheric and instrumental, not related to the parameters of interest, the atmospheric backscatter-

ing and the transmission. There are two common ways to determine the total offset component that is subtracted from the lidar signal before any further inversion of the signal is made. First, one can record the output photoreceiver signal prior to emitting the laser pulse in the atmosphere, and use this pretriggered signal as a measure of the total offset component. The second way is to determine the recorded signal at distant ranges, where the backscatter signal component decreases to zero. Neither approach is perfect [1]. Generally, the laser discharge originates electromagnetic noise in a wide spectrum, which is superimposed on the signal offset. Typically, the electromagnetic noise is a slowly decaying ringing voltage induced after triggering the light pulse [2–7]. Accordingly, the backscatter signal after the subtraction of the pretriggered signal may have some remaining constant or variable shift. In properly

assembled lidar, the shift is generally insignificant as compared with near-end values of the lidar signal. However, over distant ranges, even a minor remaining shift can yield large measurement errors, especially in clear atmosphere [8,9].

Therefore, in many cases, the determination of the offset over the far end of the recorded signal (where the backscatter component decreases to zero) may be preferable. However, in this case, any remaining non-zero backscatter component due to either the molecular or the particulate scattering can result in a systematic shift in the calculated offset. This effect does not take place when a lidar signal is recorded in the stratosphere, over altitudes of up to 70–100 km [10]. However, when working in a lower troposphere, such an effect may occur even if no particulate, but only molecular loading, exists over the distant ranges used for determining the offset component [1]. As the atmospheric molecular component depends on the wavelength, the remaining shift will be more significant for shorter wavelengths.

Here we introduce an alternative way for determining the offset over the far end of the recorded signal. The approach works if any afterpulsing effect caused by the time-dependent electronic noise is suppressed or compensated, that is, the signal offset is time independent. The method allows the exclusion of a possible shift in the calculated backscatter signal that has origins in a remaining nonzero value of the backscatter component. It was tested using both simulated and experimental data and proved to be extremely robust.

2. Method

A. Algorithm

For simplicity, we will consider the case of a ground-based and vertically pointed lidar. The original signal $P_{\Sigma}(h)$ recorded by the lidar from height h is a total of a backscatter signal $P(h)$ and an offset B :

$$P_{\Sigma}(h) = P(h) + B, \quad (1)$$

where the offset is assumed to be time independent ($B = \text{const.}$).

In the most general form, the backscatter signal $P(h)$ over a zone of the complete overlap can be written as

$$P(h) = \frac{1}{h^2} C_0 \beta_{\pi}(h) [T_t(0, h)]^2, \quad (2)$$

where C_0 is a lidar constant, $\beta_{\pi}(h)$ is the sum of the particulate and molecular backscatter coefficients $\beta_{\pi,p}(h)$ and $\beta_{\pi,m}(h)$, respectively, $[T_t(0, h)]^2$ is the total particulate and molecular two-way transmission over the distance from ground surface to h defined as

$$\begin{aligned} [T_t(0, h)]^2 &= [T_p(0, h)]^2 [T_m(0, h)]^2 \\ &= \exp \left[-2 \int_0^h \kappa_p(\xi) d\xi \right] \exp \left[-2 \int_0^h \kappa_m(\xi) d\xi \right], \end{aligned} \quad (3)$$

where $\kappa_p(h)$ and $\kappa_m(h)$ are the particulate and molecular extinction coefficients, respectively.

In a conventional signal inversion procedure, the offset B is initially determined and subtracted. After this, the backscatter signal is square-range corrected. Accordingly, for the vertically pointed lidar, the backscatter square-range-corrected signal, which is used to obtain atmospheric characteristics of interest, is calculated as

$$P(h)h^2 = [P_{\Sigma}(h) - B]h^2. \quad (4)$$

In our alternative method, a different procedure is used. The square-range-corrected procedure is initially fulfilled using the original (total) signal, $P_{\Sigma}(h)$, recorded by lidar (Eq. (1)), and only then the offset component B is determined and removed. Moreover, in addition to the square-range correction, the lidar-signal monotonic change due to the molecular component of the atmosphere is compensated. For such compensation, the vertical molecular profile should be known. The transformed signal, $Y(h) = P_{\Sigma}(h)h^2[\beta_{\pi,m}(h)]^{-1}[T_m(0, h)]^{-2}$, is calculated which, according to Eqs. (1) and (2), is the sum of two constituents:

$$\begin{aligned} Y(h) &= \frac{P_{\Sigma}(h)h^2}{\beta_{\pi,m}(h)[T_m(0, h)]^2} \\ &= C_0[1 + R_{\beta}(h)][T_p(0, h)]^2 + \frac{Bh^2}{\beta_{\pi,m}(h)[T_m(0, h)]^2}, \end{aligned} \quad (5)$$

where $R_{\beta}(h) = \beta_{\pi,p}(h)/\beta_{\pi,m}(h)$.

If one selects a restricted height interval (h_1, h_2) somewhere over the far end of the recorded signal, where a pure molecular scattering takes place, that is, $R_{\beta}(h) = 0$, and accordingly, $[T_p(0, h)]^2$ is constant, the first constituent in Eq. (5) will also be constant. Thus, for any point within this altitude range, the condition will be valid:

$$C_0[1 + R_{\beta}(h)][T_p(0, h)]^2 = A, \quad (6)$$

where A is a constant. Accordingly, Eq. (5) transforms into a linear equation:

$$Y(x) = A + Bx, \quad (7)$$

with the independent variable x defined as

$$x = \frac{h^2}{\beta_{\pi,m}(h)[T_m(0, h)]^2}. \quad (8)$$

The unknown offset B can be found from Eq. (7) as a slope of $Y(x)$ over the distant range from x_1 to x_2 . After that, the backscatter signal of interest, $P(h)$, is found in the conventional way, as the difference of $P_\Sigma(h)$ and B , and then square-range corrected [Eq. (4)].

B. Solution Uncertainty When $R_\beta(h) > 0$

In general, the estimated offset $\langle B \rangle$ will differ from the actual offset B . This effect will cause a systematic nonzero error in the retrieved backscatter signal of interest. Note that the distortion of the retrieved backscatter signal is caused by the nonzero component $\Delta B = \langle B \rangle - B$ rather than the offset B . The systematic uncertainty, $\Delta B \neq 0$, may take place if the condition of an aerosol-free atmosphere, $R_\beta(h) = 0$, is not valid for the far-end height interval (h_1, h_2) , selected for the estimation of the offset. However, when no large gradient in $R_\beta(h)$ over this interval takes place, the presence of a moderate aerosol loading is not critical. In such a case, the uncertainty in the estimate of the offset B through determining the slope of the linear fit in Eq. (7) is generally small.

A standard way to determine the slope of a function of interest is to use a least-square method [11]. However, to make clear the influence of the nonzero aerosol loading over presumably aerosol-free altitudes on the estimated offset, $\langle B \rangle$, we will apply the two-point solution method for the estimation of the constant B in Eq. (7). Particularly, we will determine the estimate $\langle B \rangle$ using data-points of the function $Y(x)$ at points x_1 and x_2 . The solution for $\langle B \rangle$ can be written then as

$$\langle B \rangle = \frac{Y(x_2) - Y(x_1)}{x_2 - x_1} = B + \frac{C_0\{[1 + R_\beta(h_2)][T_p(0, h_2)]^2 - [1 + R_\beta(h_1)][T_p(0, h_1)]^2\}}{x_2 - x_1}. \quad (9)$$

The estimate $\langle B \rangle$ is equal to the true offset B if, within the altitude range (h_1, h_2) , the ratio $R_\beta(h) = 0$ and, accordingly, $[T_p(0, h_1)]^2 = [T_p(0, h_2)]^2$. Simple transformation of Eq. (9) yields the following formula for the absolute error of the estimated offset $\Delta B = \langle B \rangle - B$:

$$\Delta B = \left[\frac{x_2}{x_2 - x_1} \right] P(h_2) - \left[\frac{x_1}{x_2 - x_1} \right] P(h_1). \quad (10)$$

Here $P(h_1)$ and $P(h_2)$ are the backscatter signals at h_1 and h_2 , which in common case include both molecular and particulate components [Eq. (2)]. Equation (10) can be rewritten in the form

$$\Delta B = P(h_1) \left(\frac{x_1}{x_2 - x_1} \right) \left\{ \left(\frac{1 + R_\beta(h_2)}{1 + R_\beta(h_1)} \right) \times \exp[-2\tau_p(h_1, h_2)] - 1 \right\}, \quad (11)$$

where $\tau_p(h_1, h_2)$ is the particulate optical depth over the selected altitude range (h_1, h_2) . As follows from Eq. (11), ΔB is small under the conditions that:

1. the interval (h_1, h_2) is properly selected, so that the backscatter signal at h_1 is small;
2. no large gradients in $R_\beta(h)$ exist within the interval (h_1, h_2) ; and
3. the particulate optical depth within the interval is small.

It is also worth mentioning that Eqs. (9)–(11) are derived using only two points for determining the slope in Eq. (7). When the commonly used standard least-squares method is applied, the error ΔB is generally significantly less.

3. Simulation

Let us consider a vertically pointed lidar that operates in simulated atmospheric conditions. In this atmosphere, the particulate extinction coefficient at the lidar wavelength 355 nm monotonically decreases with the height from $\kappa_p(h) = 0.17 \text{ km}^{-1}$ at ground level down to $\kappa_p(h) = 0.026 \text{ km}^{-1}$ at the height $h = 12,000 \text{ m}$. Also, a turbid layer with a maximum value of $\kappa_p(h) = 0.18 \text{ km}^{-1}$ exists at the heights from 900 to 1200 m. In addition, a thin cloud with the extinction coefficient $\kappa_p(h) = 0.2 \text{ km}^{-1}$ exists at the heights between 4000 and 4350 m. This model profile of $\kappa_p(h)$ is shown in Fig. 1 as the solid curve; the assumed molecular extinction-coefficient profile $\kappa_m(h)$ at 355 nm is shown as the dotted curve. The data

points of the corresponding backscatter signal $P(h)$ calculated for the lidar with a height-independent lidar ratio 20 sr and corrupted with quasi-random noise are shown in Fig. 2 as black dots.

In lidar measurements, only the value of the total signal, $P_\Sigma(h)$, which includes some unknown offset B , is commonly known. The total signal used in our numerical experiment as an input parameter was calculated as the sum of the noisy $P(h)$ and the constant offset $B = 300$ arbitrary units (a.u.). The selected constant $C_0 = 75,000$ yielded the maximum value of the total signal, $P_\Sigma(h)$ at the near end ($h = 500 \text{ m}$) equal to 4053 a.u. This value is sensible

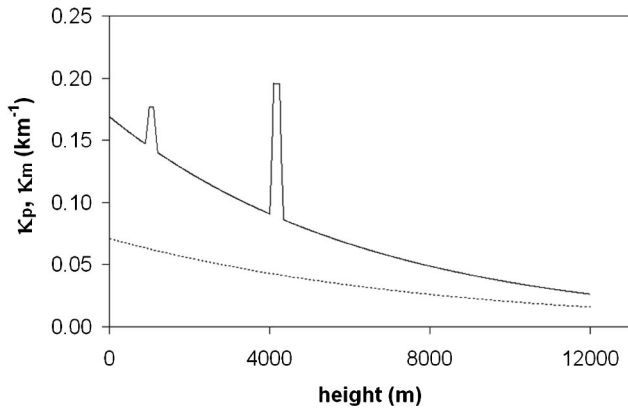


Fig. 1. Model profiles of the vertical particulate extinction coefficient (solid curve) and the molecular extinction coefficient (dotted curve) used for simulations.

assuming that a 12 bit digitizer is used for recording the data of our artificial lidar.

The estimate $\langle B \rangle$ was found as the slope of the corresponding function $Y(x)$ versus x [Eq. (7)] with the least-square method using two quite different step sizes, $s_1 = 200$ m and $s_2 = 2000$ m. The corresponding numerical derivative profiles obtained when using running mean with these step sizes are shown in Fig. 3. As can be expected, the numerical derivative calculated with the smaller step size s_1 , shown by the gray cross symbols, is significantly noisier than that obtained with the step size s_2 , shown as a solid curve. However, the mean values of these functions, calculated for the height interval 9000–11,000 m and used as the estimates of the unknown offset, proved to be quite close to each other, $\langle B(s_1) \rangle = 299.93$ a.u. and $\langle B(s_2) \rangle = 299.95$ a.u., respectively; both values are quite close to the model value, $B = 300$ a.u. The conventional way of determining the offset as a mean value of the total signal, $P_\Sigma(h)$, over the same altitude range from 9000 to 11,000 m, yielded $\langle B(P_\Sigma) \rangle = 300.25$ a.u.; it is also quite close to the true value, although it is found in the area where a small nonzero aerosol loading still exists and $R_\beta(h) \neq 0$.

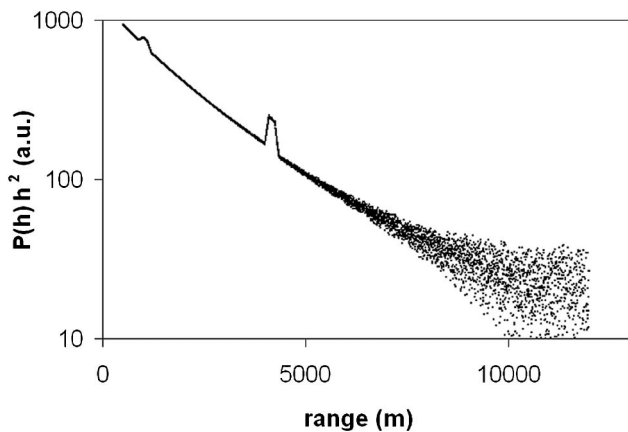


Fig. 2. Noise-corrupted profile of the square-range-corrected signal of a ground-based lidar versus height calculated for the model atmosphere in Fig. 1.

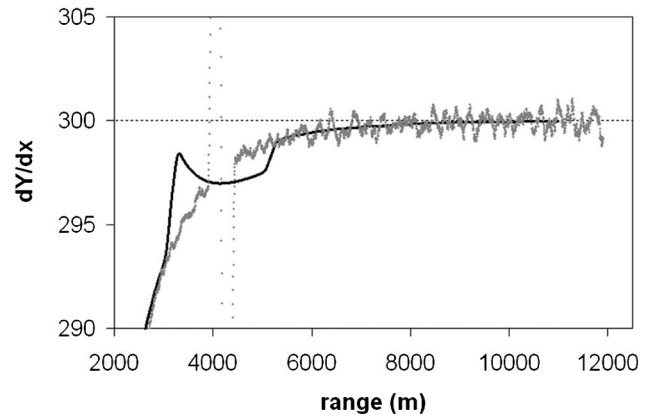


Fig. 3. Range-resolved profiles of dY/dx obtained using the numerical differentiation of Eq. (7) with the running mean. The gray cross symbols show the derivative profile obtained with $s_1 = 200$ m and the thick curve shows that obtained with $s_2 = 2000$ m. The dotted horizontal line shows the actual signal offset $B = 300$ a.u.

Note that both $\langle B(s_1) \rangle$ and $\langle B(s_2) \rangle$ are less than the “true” offset, $B = 300$ a.u., whereas $\langle B(P_\Sigma) \rangle > B$. We will show below that the systematic difference between $\langle B(s) \rangle$ and $\langle B(P_\Sigma) \rangle$ is a very useful specific of our alternative method.

In Fig. 4, the range-corrected signals $P(h)h^2$ over a far end are shown determined from the data points of the noisy signal $P_\Sigma(h)$ averaged over the height interval of 100 m. The profiles of the square-range-corrected signals, shown as curves 1, 2, and 3, were obtained with the above offset estimates, $\langle B(s_1) \rangle$, $\langle B(s_2) \rangle$, and $\langle B(P_\Sigma) \rangle$, respectively. For comparison, the model signal $P(h)h^2$ not corrupted by noise is also shown (curve 4). One can see that the data points, calculated with the estimate $\langle B(P_\Sigma) \rangle$, are smaller than the model signal $P(h)h^2$. They even become negative over heights more than 10,000 m, whereas the signals, retrieved with the estimates $\langle B(s_1) \rangle$ and $\langle B(s_2) \rangle$, are positive and a little larger than the model signal. These shifts are systematic. The appearance of negative values of $P(h)h^2$ over the far ranges when

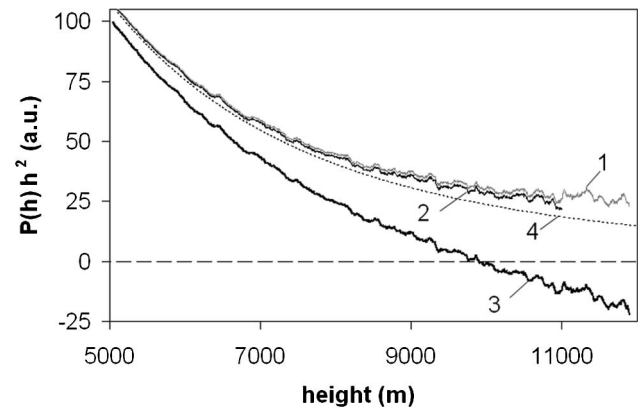


Fig. 4. Height-corrected signals $P(h)h^2$ determined from the noise-corrupted signal $P_\Sigma(h) = P(h) + B$ using the estimates $\langle B(s_1) \rangle$, $\langle B(s_2) \rangle$, and $\langle B(P_\Sigma) \rangle$ (the curves 1, 2, and 3, respectively). The model range-corrected signal, not corrupted by noise, is shown as curve 4.

using the estimate $\langle B(P_\Sigma) \rangle$ is due to ignoring the molecular component of the atmosphere over the height interval where the estimation of the offset is made. Note that the initial shifts $\Delta P(h)$ in the signal $P(h)$ for the selected range from 9000–11,000 m are minor; they are within the range ± 0.2 a.u.

The increased values of $P(h)h^2$, obtained when using the estimates $\langle B(s_1) \rangle$ and $\langle B(s_2) \rangle$, require clarification: in some special cases, the signal shift may be negative, and this should be checked when performing calculations. Simple algebraic transformation of Eq. (10) shows that the shift remaining in the lidar signal, $\Delta P = B - \langle B(s) \rangle$, is positive when the simple inequality is true:

$$\frac{P(h_2)}{P(h_1)} < \frac{x_1}{x_2}. \quad (12)$$

This inequality can be violated in areas of inhomogeneous layers, in the above case, for example, over the height interval centered close to 4000 m. Note that, in such areas, the numerical derivatives, determined with different step sizes, significantly differ from each other (Fig. 3). This is an additional constraint when selecting the height interval for determining the background offset via the slope of $Y(x)$ versus x in Eq. (7). Under the above condition in Eq. (12), $\langle B(s) \rangle \leq B$, and the remaining shift ΔP in the signal $P(h)$ will be positive. Meanwhile, the shift ΔP in the signal $P(h)$ is negative when the offset B is estimated through determining the total signal $P_\Sigma(h)$ over high altitudes because $\langle B(P_\Sigma) \rangle \geq B$. In the practical sense, the different signs of the shifts $\langle B(s) \rangle$ and $\langle B(P_\Sigma) \rangle$ can allow some estimation of possible upper and lower uncertainty limits in calculated $P(h)$ and, accordingly, in the square-range-corrected signal $P(h)h^2$ caused by the uncertainty in the estimated offset. This phenomenon, in turn, gives a unique opportunity to estimate the uncertainty in the retrieved extinction-coefficient profile, for example, when utilizing the most commonly used far-end lidar-equation solution. Until now, only the level of signal random noise is generally taken into consideration when estimating the uncertainty of the far-end solution [12]. This drawback may result in the overestimated accuracy of the retrieved extinction-coefficient profile.

In Fig. 5, two vertical profiles of particulate extinction-coefficient are shown, retrieved from the above-simulated lidar signals with the Klett's far-end solution. The far-end boundary point is selected at the range $r_b = 8000$ m. It is assumed that all the boundary conditions at r_b are precisely known, so the introduced measurement error is solely due to the constant nonzero shift remaining in the lidar signal after subtracting the estimated total offset. The thick curve is the extinction-coefficient profile obtained when the above estimate $\langle B(P_\Sigma) \rangle = 300.25$ a.u. is used. The thin solid curve shows the profile derived with the estimate $\langle B(s_1) \rangle = 299.93$ a.u. [The profile derived with another estimate, $\langle B(s_2) \rangle$, practically coincides with that obtained with $\langle B(s_1) \rangle$ and, there-

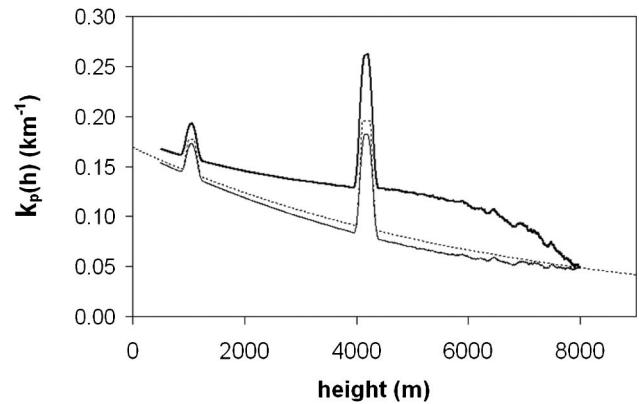


Fig. 5. Vertical profiles of particulate extinction coefficient retrieved with the far-end solution using the estimates $\langle B(s_1) \rangle$ and $\langle B(P_\Sigma) \rangle$ (the thin and thick solid curves, respectively). The dotted curve shows the “actual” (model) profile.

fore, is not shown in the figure.] The model profile of the extinction coefficient is shown as the dotted curve. Note that even the small signal shift, $\Delta P = -0.25$ a.u., which takes place when using the estimate $\langle B(P_\Sigma) \rangle$, causes the large error in the retrieved extinction coefficient, 50% and more. The error obtained with the estimates $\langle B(s_1) \rangle$ or $\langle B(s_2) \rangle$ is much lower.

4. Determination of Total Lidar-Signal Offset and Uncertainty Limits in Multiangle Measurements

As follows from Section 3, even large distortions in the extinction-coefficient profile caused by a systematic lidar-signal shift are generally “not visible” in the retrieved data of one-directional lidar measurement. To the contrary, multiangle measurements immediately show the presence of the lidar-signal distortions by yielding unrealistic profiles of the retrieved optical parameters. Inverting the multiangle data is always an issue, even in a well-horizontally stratified atmosphere, because the inversion results are extremely sensitive to any lidar-signal systematic distortion [8]. Here the main issue is to remove or compensate the signal distortions, rather than reveal them, as in one-directional measurements.

In this section, we analyze the specifics in the estimation of the uncertainty limits due to remaining systematic shifts ΔP in the lidar signals when performing multiangle measurements. The inversion results shown below were retrieved from the signals at 355 nm measured during a clear sunny day on 16 August 2008, in the vicinity of Missoula, Montana. The measurements were made in a combined slope–azimuthal mode [9], where 12 fixed slopes in the elevation range from 7.5° to 68° were used. For each azimuthally averaged signal, two algorithms were used when determining the total offset. First, the total offset $\langle B(s) \rangle$ was calculated, as described in Section 2, using two different step sizes s . Second, the offset $\langle B(P_\Sigma) \rangle$ was determined by calculating the average of the signal $P_\Sigma(r)$ over the far end of the measured range.

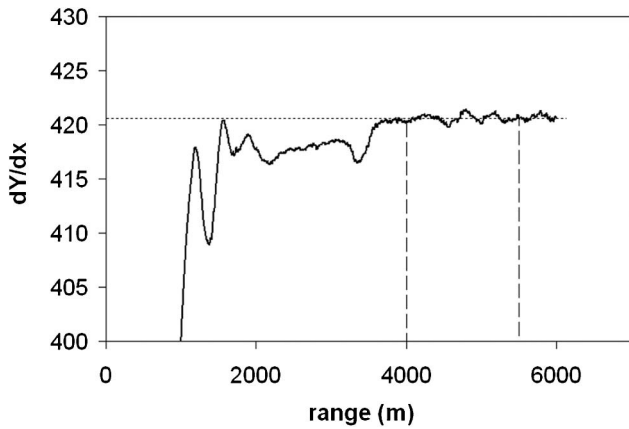


Fig. 6. Derivative of $Y(x)$ versus x calculated for the lidar signal $P_{\Sigma}(r)$ azimuthally averaged over the elevation 32° (solid curve). The offset, $\langle B(s) \rangle$, determined as the average of the function over the range from 4000 to 5500 m, is shown as the horizontal dotted line.

Figures 6 and 7 illustrate typical results obtained from the azimuthally averaged signals $P_{\Sigma}(r)$ measured at a fixed elevation. The numerical derivative of the function $Y(x)$ versus x , obtained from the signal, is shown in Fig. 6 as the thick solid curve. The numerical differentiation was performed using the running least-squares method with the step size $s = 300$ m. The offset estimate $\langle B(s) \rangle = 420.61$ a.u. was determined as the average of the derivative over the range from 4000 to 5500 m. The same as in the above simulations, we obtained quite close values of $\langle B(s) \rangle$ when using significantly different step sizes s . The offset $\langle B(P_{\Sigma}) \rangle$, determined by calculating an average of the signal $P_{\Sigma}(r)$ at the far end of the measured range, over the range from $r = 5640$ m to $r = 6140$ m, yielded the value of $\langle B(P_{\Sigma}) \rangle = 421.26$ a.u. After that, the corresponding signals, $P_1(r) = P_{\Sigma}(r) - \langle B(s) \rangle$ and $P_2(r) = P_{\Sigma}(r) - \langle B(P_{\Sigma}) \rangle$, were calculated and then square-range corrected. In Fig. 7, the signals $P_1(r)r^2$ and $P_2(r)r^2$ are shown as black dots and gray squares, respectively. Note

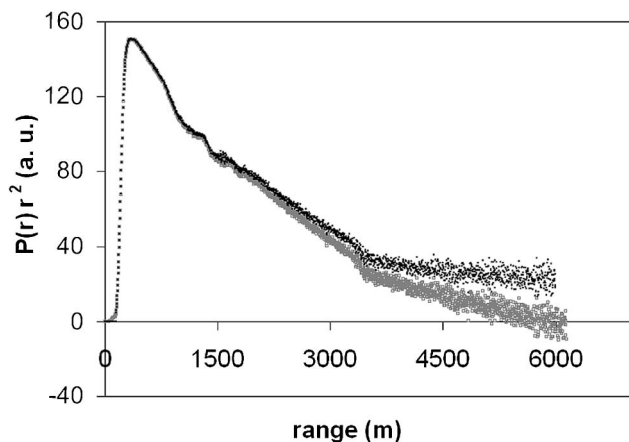


Fig. 7. Square-range-corrected signals versus range for the elevation 32° . Black dots show the signal calculated using the estimate $\langle B(s) \rangle = 420.61$ a.u. and the gray squares show that obtained with $\langle B(P_{\Sigma}) \rangle = 421.26$ a.u.

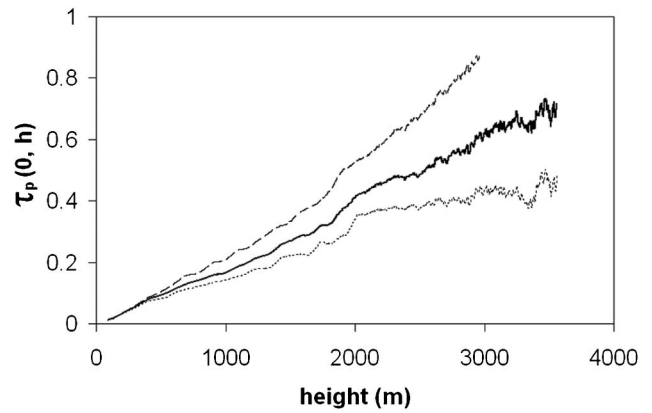


Fig. 8. Dependence of particulate optical depth on the height calculated using different methods for the estimation of the total signal offsets. The dotted curve shows the optical depth obtained from signals for which the estimate $\langle B(s) \rangle$ was used for the azimuthally averaged signals, the dashed curve shows that obtained with the estimate $\langle B(P_{\Sigma}) \rangle$, and the solid curve shows the profile obtained when using an average of $\langle B(s) \rangle$ and $\langle B(P_{\Sigma}) \rangle$.

that, in spite of the minor difference between $\langle B(P_{\Sigma}) \rangle$ and $\langle B(s) \rangle$ of 0.65 a.u., the difference in the shape of the signals $P_1(r)r^2$ and $P_2(r)r^2$ for the distant ranges, $r > 3000$ m, is significant.

A thorough data analysis of the whole scan over 12 fixed slopes confirmed that, in all signals, $\langle B(s) \rangle < \langle B(P_{\Sigma}) \rangle$, and the difference between these values is small, ranging from 0.65 to 1.11 a.u., which is less than 0.3% from the estimated signal offset. Nevertheless, even such a minor difference significantly influences the result of the multiangle lidar-signal inversion. In Fig. 8, the vertical particulate optical depth $\tau_p(0, h)$ versus height is shown calculated with the above two methods of the estimation of the total signal offset. The dotted curve shows the optical depth obtained when using the estimate $\langle B(s) \rangle$, and the dashed curve shows the optical depth obtained with the estimate $\langle B(P_{\Sigma}) \rangle$. These curves allow some estimation of possible upper and lower uncertainty boundaries in the retrieved optical depth caused by the uncertainty in the estimate of the offset B . Such an estimation of the uncertainty boundaries is quite useful, for example, when the method of inverting lidar multiangle data considered in [13] is utilized. The solid curve shows a mean profile, obtained when using an average of $\langle B(s) \rangle$ and $\langle B(P_{\Sigma}) \rangle$ as an estimate of the signal offset. One should always keep in mind that the behavior of such profiles, retrieved from multiangle measurements, depends on the selection of the maximum range for the signal; this is a significant issue when utilizing the angle-dependent lidar equation.

5. Summary

The original signal recorded by lidar is the total of the attenuated range-dependent backscatter signal and a constant offset. The offset is created by a background component and a recording system electronic offset. The retrieval of optical characteristics of the aerosol particulates from lidar data

requires the separation and removal of the offset component from the recorded signal. It is not possible to estimate the constant offset with zero uncertainty. Meanwhile, even a minor shift remaining in the signal after the subtraction of the estimated offset can result in significant systematic distortions in the inversion results of both the one-directional and multi-angle methods.

We presented a new principle for determining the total offset in the lidar signal created by a daytime background-illumination and electrical or digital offsets. The method is compared with the conventional method of offset determination via determining the level of the recorded signal over distant ranges where the backscatter signal is presumably zero.

It is shown that the simultaneous use of the alternative and the conventional techniques for determining the total offset in lidar signals can allow estimation of possible limits in the systematic shift in the inverted backscatter signal caused by uncertainty in the estimated signal offset. This technique gives an opportunity for the estimation of the uncertainty limits in the inverted lidar signals when utilizing a one-directional measurement, and the upper and lower uncertainty limits in the retrieved optical depth in the multiangle measurement. Taking into consideration the distorting effect of the remaining shift in the lidar signal will prevent overestimating the accuracy of the retrieved atmospheric parameters of interest, as may happen when only statistical error is considered.

References

1. V. A. Kovalev, "Distortion of the extinction coefficient profile caused by systematic errors in lidar data," *Appl. Opt.* **43**, 3191–3198 (2004).
2. S. R. Ahmad and E. M. Bulliet, "Performance evaluation of a laboratory-based Raman lidar in atmospheric pollution measurement," *Opt. Laser Technol.* **26**, 323–331 (1994).
3. H. Shimizu, Y. Sasano, H. Nakane, N. Sugimoto, I. Matsui, and N. Takeuchi, "Large-scale laser radar for measuring aerosol distribution over a wide area," *Appl. Opt.* **24**, 617–626 (1985).
4. Y. Zhao, "Signal-induced fluorescence in photomultipliers in differential absorption lidar systems," *Appl. Opt.* **38**, 4639–4648 (1999).
5. J. A. Sunesson, A. Apituley, and D. P. J. Swart, "Differential absorption lidar system for routine monitoring of tropospheric ozone," *Appl. Opt.* **33**, 7045–7058 (1994).
6. H. S. Lee, G. K. Schwemmer, C. L. Korb, M. Dombrowski, and C. Prasad, "Gated photomultiplier response characterization for DIAL measurements," *Appl. Opt.* **29**, 3303–3315 (1990).
7. M. Bristow, "Suppression of afterpulsing in photomultipliers by gating the photocathode," *Appl. Opt.* **41**, 4975–4987 (2002).
8. V. A. Kovalev, W. M. Hao, C. Wold, and M. Adam, "Experimental method for the examination of systematic distortions in lidar data," *Appl. Opt.* **46**, 6710–6718 (2007).
9. M. Adam, V. A. Kovalev, C. Wold, J. Newton, M. Pahlow, Wei M. Hao, and M. B. Parlange, "Application of the Kano–Hamilton multiangle inversion method in clear atmospheres," *J. Atmos. Ocean. Technol.* **24**, 2014–2028 (2007).
10. O. Uchino and I. Tabata, "Mobile lidar for simultaneous measurements of ozone, aerosols, and temperature in the stratosphere," *Appl. Opt.* **30**, 2005–2012 (1991).
11. J. R. Taylor, *An Introduction to Error Analysis. the Study of Uncertainties in Physical Measurements* (University Science Books, 1997).
12. A. Comeron, F. Rocadenbosch, M. A. Lopez, A. Rodriguez, C. Munoz, D. Garcia-Vizcaino, and M. Sicard, "Effects of noise on lidar data inversion with the backward algorithm," *Appl. Opt.* **43**, 2572–2577 (2004).
13. V. A. Kovalev, W. M. Hao, and C. Wold, "Determination of the particulate extinction-coefficient profile and the column-integrated lidar ratios using the backscatter-coefficient and optical-depth profiles," *Appl. Opt.* **46**, 8627–8634 (2007).